

Deep Learning for Highly Accelerated Diffusion Tensor Imaging

Hongyu Li¹, Zifei Liang², Chaoyi Zhang¹, Ruiying Liu¹, Jing Li³, Weihong Zhang³, Dong Liang⁴, Bowen Shen⁵, Xiaoliang Zhang¹, Yulin Ge², Jiangyang Zhang^{2*}, and Leslie Ying^{1*}

Abstract—Diffusion tensor imaging (DTI) is widely used to examine the human brain white matter structures, including their microarchitecture integrity and spatial fiber tract trajectories, with clinical applications in several neurological disorders and neurosurgical guidance. However, a major factor that prevents DTI from being incorporated in clinical routines is its long scan time due to the acquisition of a large number (typically 30 or more) of diffusion-weighted images (DWIs) required for reliable tensor estimation. Here, a deep learning-based technique is developed to obtain diffusion tensor images with only six DWIs, resulting in a significant reduction in imaging time. The method uses deep convolutional neural networks to learn the highly nonlinear relationship between DWIs and several tensor-derived maps, bypassing the conventional tensor fitting procedure, which is well known to be highly susceptible to noises in DWIs. The performance of the method was evaluated using DWI datasets from the Human Connectome Project and patients with ischemic stroke. Our results demonstrate that the proposed technique is able to generate quantitative maps of good quality fractional anisotropy (FA) and mean diffusivity (MD), as well as the fiber tractography from as few as six DWIs. The proposed method achieves a quantification error of less than 5% in all regions of interest of

the brain, which is the rate of in vivo reproducibility of diffusion tensor imaging. Tractography reconstruction is also comparable to the ground truth obtained from 90 DWIs. In addition, we also demonstrate that the neural network trained on healthy volunteers can be directly applied/tested on stroke patients' DWIs data without compromising the lesion detectability. Such a significant reduction in scan time will allow inclusion of DTI into clinical routine for many potential applications.

Index Term—Diffusion tensor imaging (DTI), diffusion-weighted images (DWIs), deep convolutional neural networks, fractional anisotropy (FA), mean diffusivity (MD), fiber tractography.

1. Department of Biomedical Engineering, Department of Electrical Engineering, University at Buffalo, the State University of New York, Buffalo, New York, USA

2. Center for Biomedical Imaging, Department of Radiology, New York University School of Medicine, New York, USA

3. Department of Radiology, Peking Union Medical College Hospital, Beijing, China

4. Paul C. Lauterbur Research Center for Biomedical Imaging, Medical AI research center, SIAT, CAS, Shenzhen, P.R.China

5. Department of Computer Science, Virginia Tech, Blacksburg, VA, USA

*Corresponding authors: Jiangyang.Zhang@nyulangone.org, leiying@buffalo.edu

I. INTRODUCTION

Diffusion-weighted imaging (DWI) uses diffusion sensitizing gradients to measure the extent of water molecule diffusion along the gradient direction [1-3]. DWI has shown to be very useful for early detection of ischemic stroke [4, 5], as well as other brain diseases, such as multiple sclerosis [6-8], trauma [9, 10], brain tumors [11, 12], and hypertensive encephalopathy [13, 14]. To account for complex patterns of water diffusion shaped by tissue microstructural

organization, e.g., anisotropic diffusion in white matter structures, diffusion tensor imaging (DTI) was later developed to characterize three-dimensional tissue water diffusion using a second-order diffusion tensor model [15]. From diffusion tensor data, several markers, such as mean diffusivity (MD) and fractional anisotropy (FA), can be derived and are widely used to visualize microstructural organizations in the brain as the diffusion tensor itself, a three-by-three matrix, is difficult to display. For example, in the white matter,

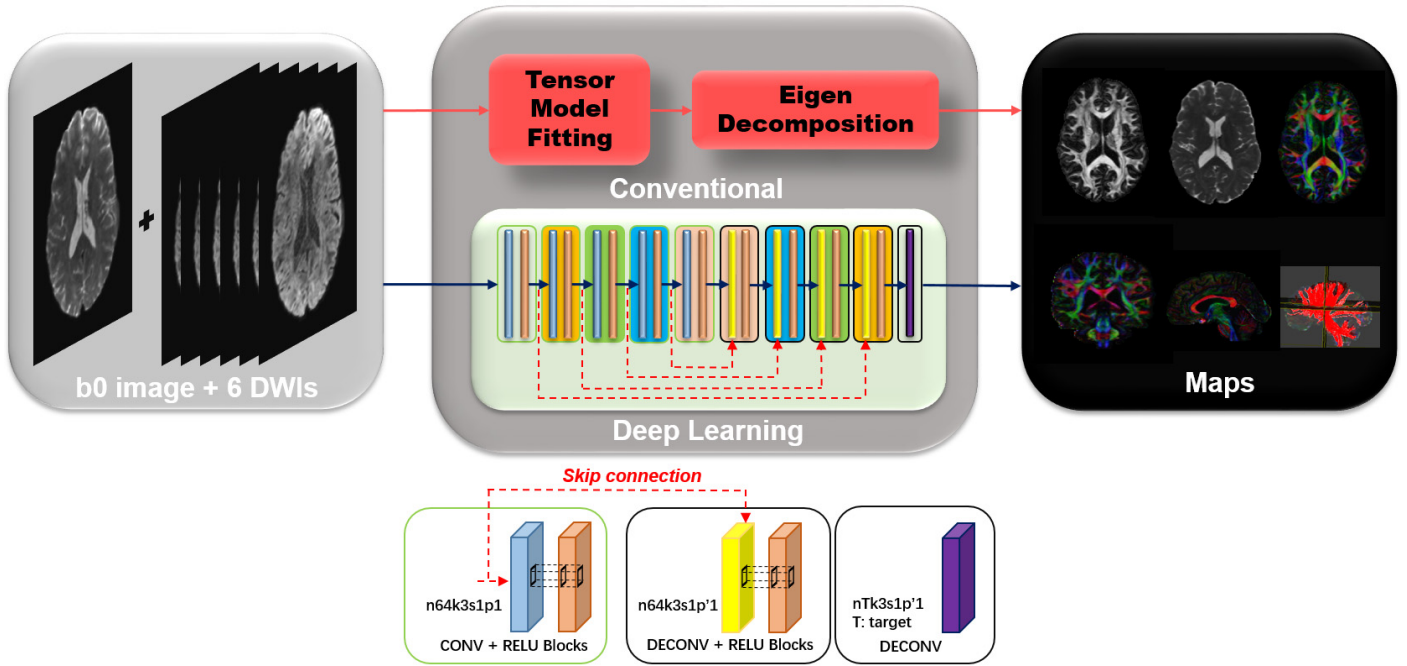


Fig. 1. Schematic comparison of the conventional DTI model fitting and deep learning methods for generating various diffusion quantification maps. In the deep learning method, CNN uses an input layer, an output layer, and multiple hidden layers of nodes to form a hierarchical structure. The proposed network comprises several layers of a skip-connection-based convolution-deconvolution network which learns the residual between its input and output. In each layer, $n64k3s1p1$ ($p'1$) indicates 64 filters of kernel size 3×3 with a stride of 1 and padding of 1 (truncation of 1). Except for the last layer, each (de)convolutional layer is followed by a ReLU unit.

the diffusion of water molecules is often restricted in the direction perpendicular to the axons by axonal membrane and myelin, leading to diffusion anisotropy [16, 17], which is sensitive to axonal and myelin injuries [18, 19]. Furthermore, the 3D directional anisotropy information encoded in diffusion tensors allows non-invasive reconstruction of the trajectories of major white matter tracts in the brain [20]. Although more sophisticated diffusion MRI techniques, such as diffusion kurtosis imaging [21] and high angular resolution diffusion imaging (HARDI)[22], have been developed to provide more comprehensive information on tissue microstructure (e.g., non-Gaussian diffusion and fiber crossing), DTI remains an important tool for neuroscience research with a wide array of clinical applications.

Although DTI theoretically requires only six diffusion-weighted images and one non-diffusion-weighted image for estimation of the diffusion tensors, many more diffusion-weighted images with different diffusion encoding directions are acquired in practice due to the low SNR and high sensitivity of the tensor model to noise contamination. For example, 30 DWIs are typically needed to obtain MDs and FAs with diagnostic quality, resulting in a scan time of 10-

30 minutes. Such a prolonged scan time can increase motion artifacts and patient's discomfort and is a major reason why DTI is not in standard clinical practice yet. Several techniques have been developed to accelerate DTI, such as parallel imaging with phased array coils, simultaneous multislice (SMS) acquisition [23], and compressed sensing [24-29]. However, the acceleration factor is limited to 2-3 with the latter involving extensive computation power.

Here we report a deep learning approach to dramatically shorten the acquisition time of DTI. This approach can be applied on top of SMS and requires little online computation once the training is completed offline. Similar to [30], we used deep convolutional neural networks to model the nonlinear relationship between acquired DWIs and desired DTI derived maps, and the speed improvement was achieved by reducing the number of required DWIs. Using data from the HCP database, we investigated whether highly accelerated (up to 15 times faster) DTI can still maintain the quality of the output maps, especially the ability to reconstruct major fiber pathways in the brain. Furthermore, we used data from patients with acute ischemic stroke to test whether networks trained using healthy subjects can potentially be applied to patients.

II. RESULTS

A. FA and MD Maps

Figure 1 shows the basic architecture of the convoluted neural networks used in this study. The network consisted of an input layer, an output layer, and multiple hidden layers of nodes to form a hierarchical structure [31, 32]. Each node of a layer is connected to some nodes of the previous layer by a linear convolution, a nonlinear activation, or a pooling (reduction from multiple to one) process. Such a hierarchical structure with deep layers can represent highly complex nonlinear models [33, 34], with different network parameters representing different models. The networks were trained using diffusion MRI data ($n=40$) from the HCP dataset.

Figure 2 shows representative FA maps, respectively, from 6, 18 and 36 DWIs generated using the conventional tensor model fitting (MF) method and proposed deep learning (DL) method from the testing dataset ($n=10$). Figure 3 plots the average mean values/MSE for FA at several ROIs in gray matter structures, subcortical and major white matter structures for the total 10 testing datasets. Figure 4 shows representative MD maps from 3, 6, 18 and 36 DWIs using MF and DL. Results from model fitting using all 90 DWIs plus 18 non-weighted images were used as the ground truth. While the model

fitting results became increasingly noisy as the number of input DWIs decreased, as expected, the FA maps generated by our deep learning method showed no apparent degradation even with only 6 DWIs. The reconstruction of MF/DL generated FA/MD maps were measured using peak signal-to-noise ratio (PSNR), which shows good performance for DL even with only 6 DWIs for FA and 3 DWIs for MD maps. It is seen that differences between MF and DL-generated MD maps were less apparent than FA maps, as MD is less sensitive to noise than FA.

Within regions of interests defined in the cortical gray matters, subcortical and major white matter structures, the FA values estimated from limited DWIs using deep learning also showed significant less deviation from the ground truth than model fitting. When only 6 DWIs were available, the conventional model-fitting method significantly over-estimates the FA values, whereas the deep learning method has MSE below 0.5% for GM structures, below 1% for subcortical WM structures, and below 1.5% for major WM structures. When 18 and more DWIs were available, the deep learning method provides consistently more accurate FA values than model fitting.

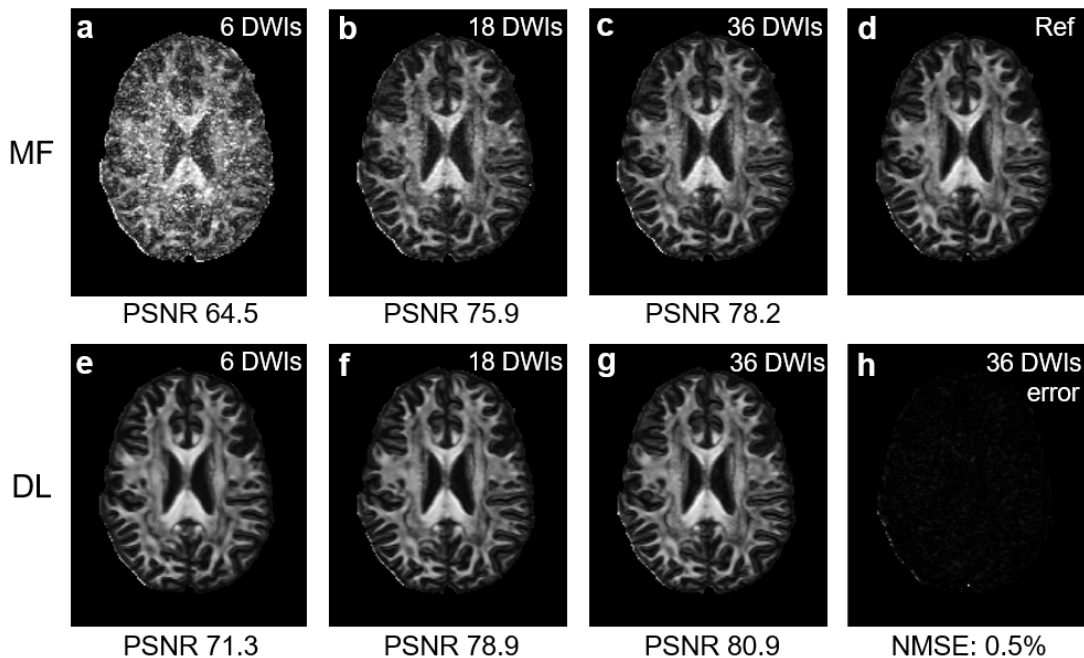


Fig. 2. FA maps from conventional tensor model fitting (MF) and the proposed deep learning methods (DL). MF generated FA maps (a-c) and DL generated FA maps (e-g) from 6, 18, and 36 DWIs. h, difference map by proposed method from 36 DWIs. The PSNRs and NMSE were calculated with the model fitted FA map from 90 DWIs (d) as the reference.

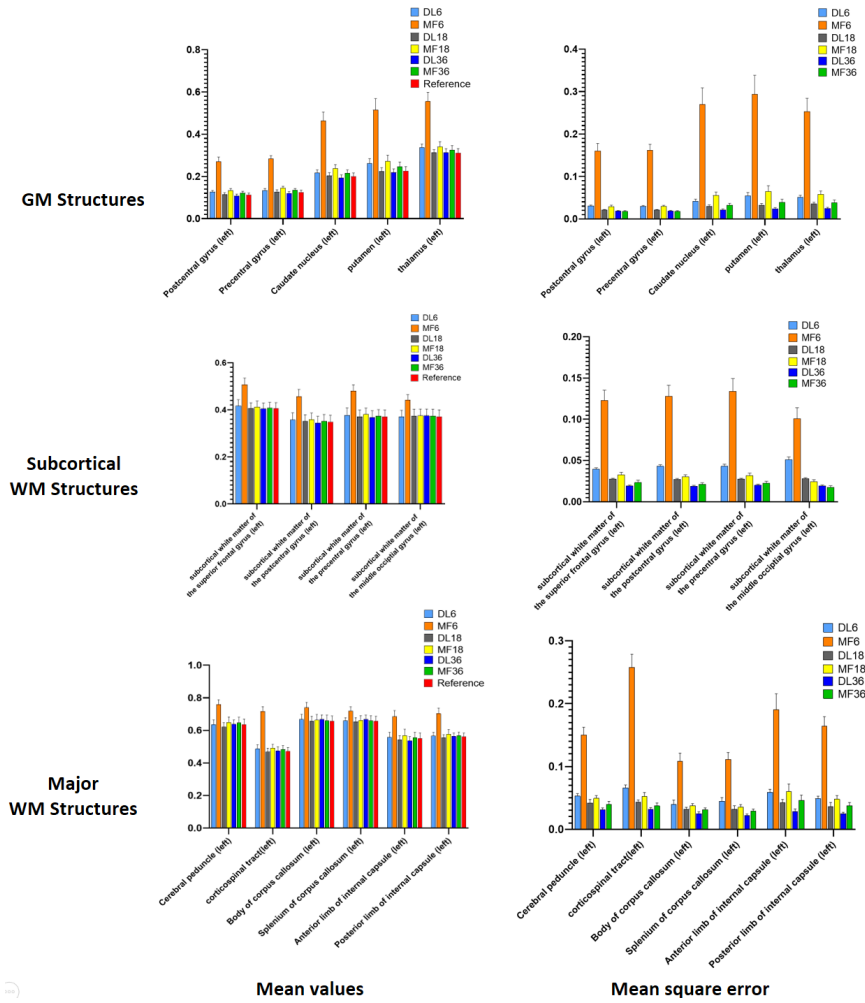


Fig. 3. Comparison of mean FA values and the corresponding MSEs. Values and errors were obtained by DL and MF with 6, 18, and 36 DWIs for different ROIs.

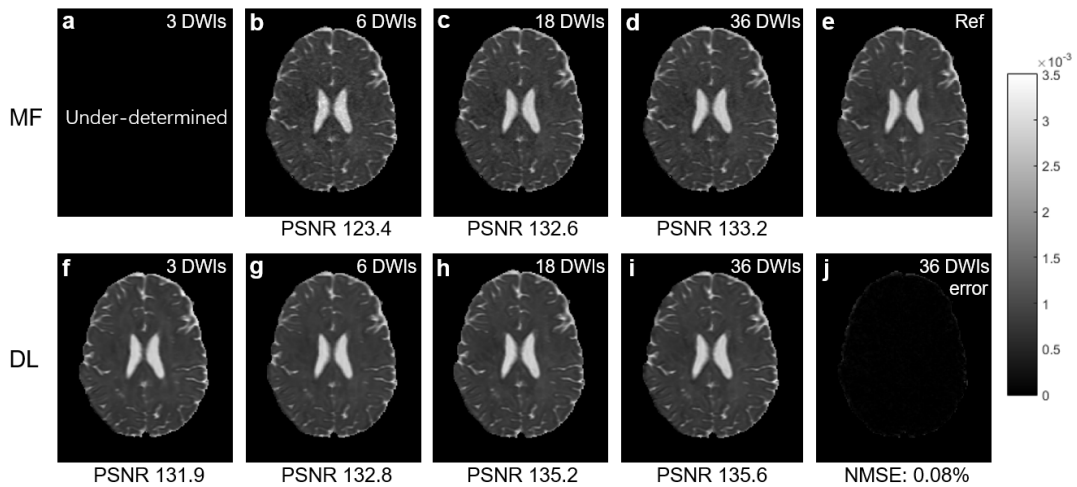


Fig. 4. MD maps. 3, 6, 18, and 36 DWIs generated MD maps by MF (a-d) and by DL (f-i). j, difference map of 36 DWIs by proposed method. The PSNRs and NMSE were calculated with the model fitted MD map from 90 DWIs (e) as the reference.

B. Directionally encoded colormap and fiber tracking

The primary eigen-vectors from a diffusion tensor indicates the principle orientation of water molecule diffusion. In combination with FA, the primary eigen-vectors can be used to generate directionally encoded colormap, which is useful to inspect 3D orientation information encoded in diffusion tensors, as well as fiber tracking. Our deep learning network can also be trained to estimate primary eigen-vectors directly from DWIs without model fitting. Figures 5 show the directionally encoded colormap and tracts generated from the eigenvectors using both deep learning and the

conventional model-fitting methods. Visually, the directionally encoded colormaps generated using deep learning results tend to maintain its quality better than model fitting with small number of DWIs. Even with only 6 DWIS, the estimated orientation of the corpus callosum remain consistently along the medial-lateral orientation (red) in the deep learning results, whereas the model fitting results showed more speckles due to erroneous estimates. Fiber tracking results based on deep learning generated FA and eigen-vectors better preserved the morphology of three major white matter tracts in the brain.

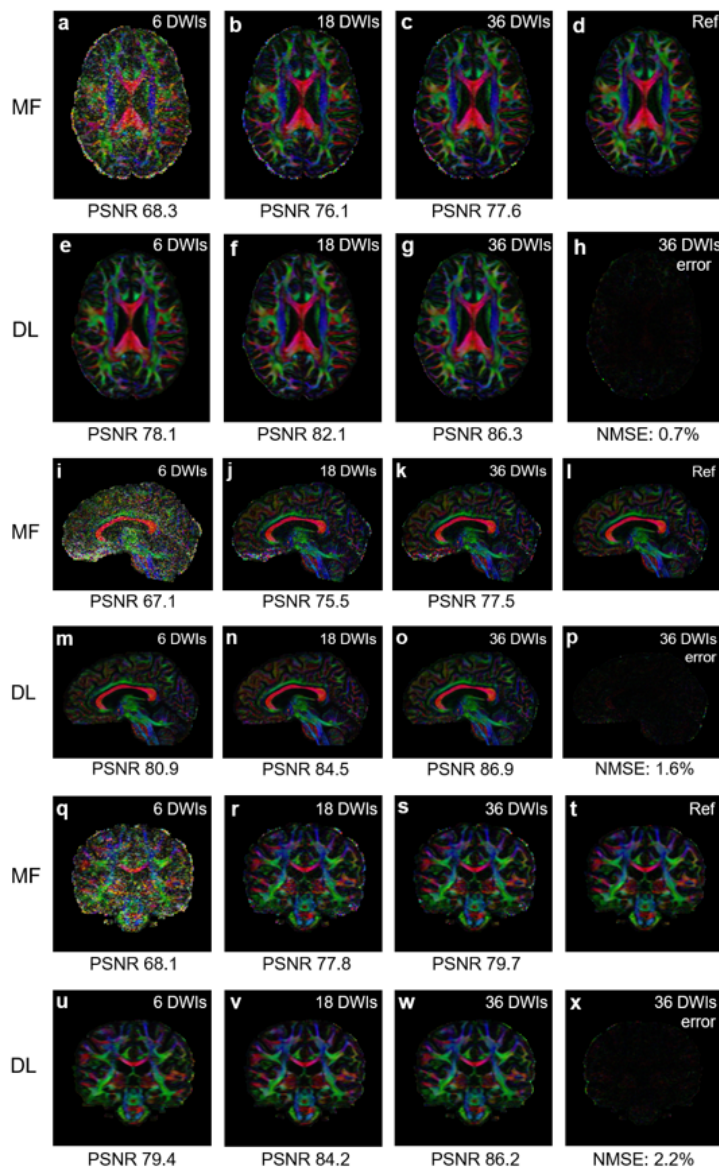


Fig. 5. Color-coded FA maps. Axial, sagittal, and coronal views by MF **a-c, i-k, q-s** and by proposed DL **e-g, m-o, u-w** from 6, 18 and 36 DWIs. **h, p** and **x** show the difference map of 36 DWIs by proposed method. The PSNRs and NMSEs were calculated with the model fitted color-maps from 90 DWIs (**d, l, t**) as the reference.

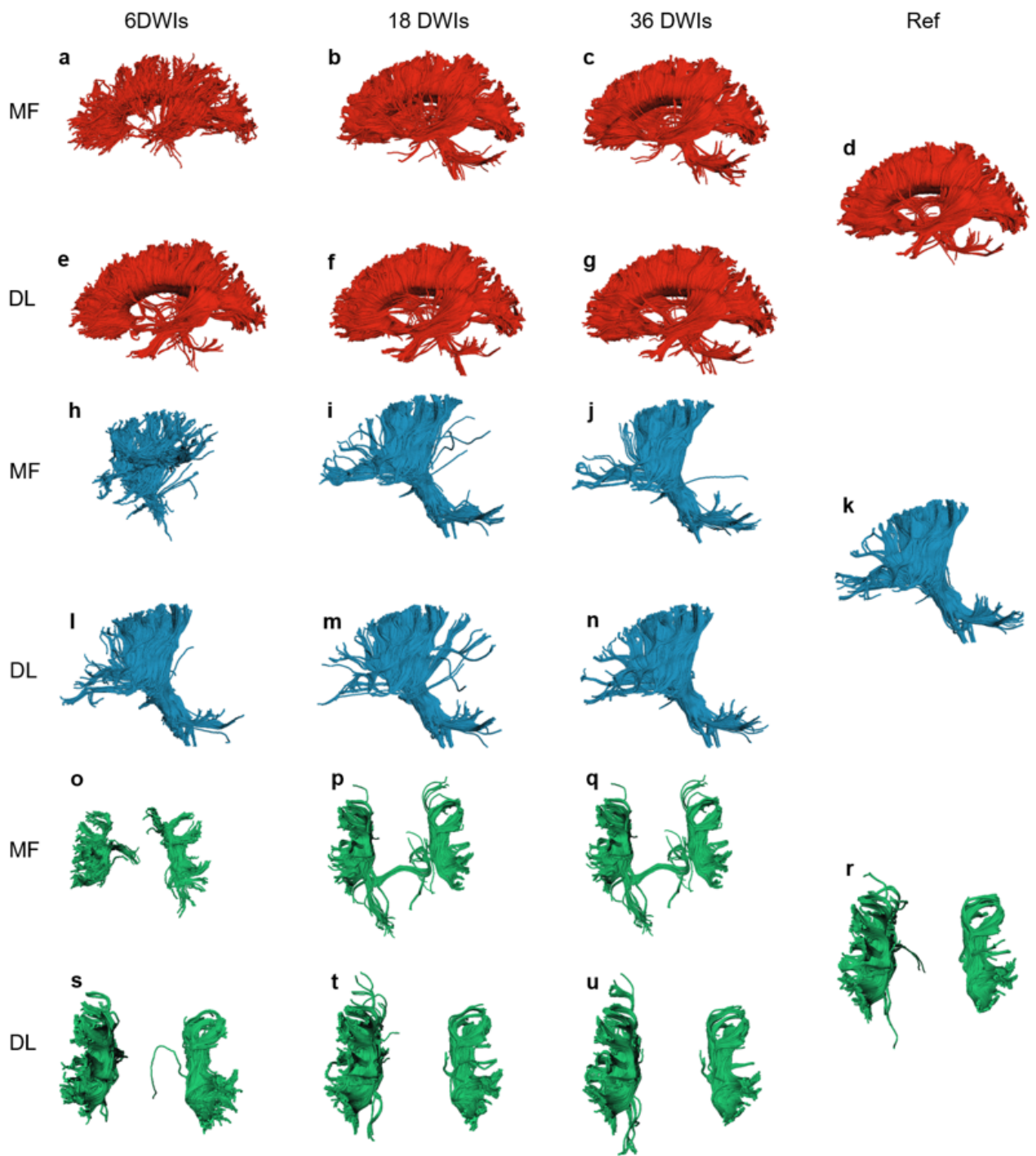


Fig. 6. Tractography. Corpus callosum **a-c** by MF, **e-g** by DL. Internal capsule/corticospinal tract (**h-j** by MF, **l-n** by DL). Superior longitudinal fasciculus (**o-q** by MF, **s-u** by DL) from 6, 18, and 36 DWIs. The model-fitted tractography from 90 DWIs (**d, k, r**) are also shown as reference.

TABLE I. STATISTICAL INFORMATION

DWIs		3		6		18		36		No.	D.
Method		DL	MF	DL	MF	DL	MF	DL	MF	Subjects	Freedom
FA	<i>pcc</i>	-	-	0.9850	0.9403	0.9916	0.9815	0.9930	0.9890	10	-
	<i>t-value</i>	-	-	0.3326	33.0802	0.3314	4.0938	0.1942	1.8505	10	18
	<i>ANOVA F-statistic</i>	-		1049.34		22.26		8.28		10	27
	<i>ANOVA p-value</i>	-		2.53e-26		1.94e-6		0.0016		10	27
MD	<i>pcc</i>	0.9982	-	0.9987	0.8783	0.9989	0.9691	0.9992	0.9850	10	-
	<i>t-value</i>	0.5132	-	0.4352	0.7932	0.4196	1.7849	0.0439	0.9808	10	18
	<i>ANOVA F-statistic</i>	-		0.1		4.59		2.79		10	27
	<i>ANOVA p-value</i>	-		0.9051		0.0192		0.0789		10	27

Pearson Correlation Coefficient, Student's T-test and ANOVA of proposed deep learning (DL) and conventional tensor model fitting (MF) methods.

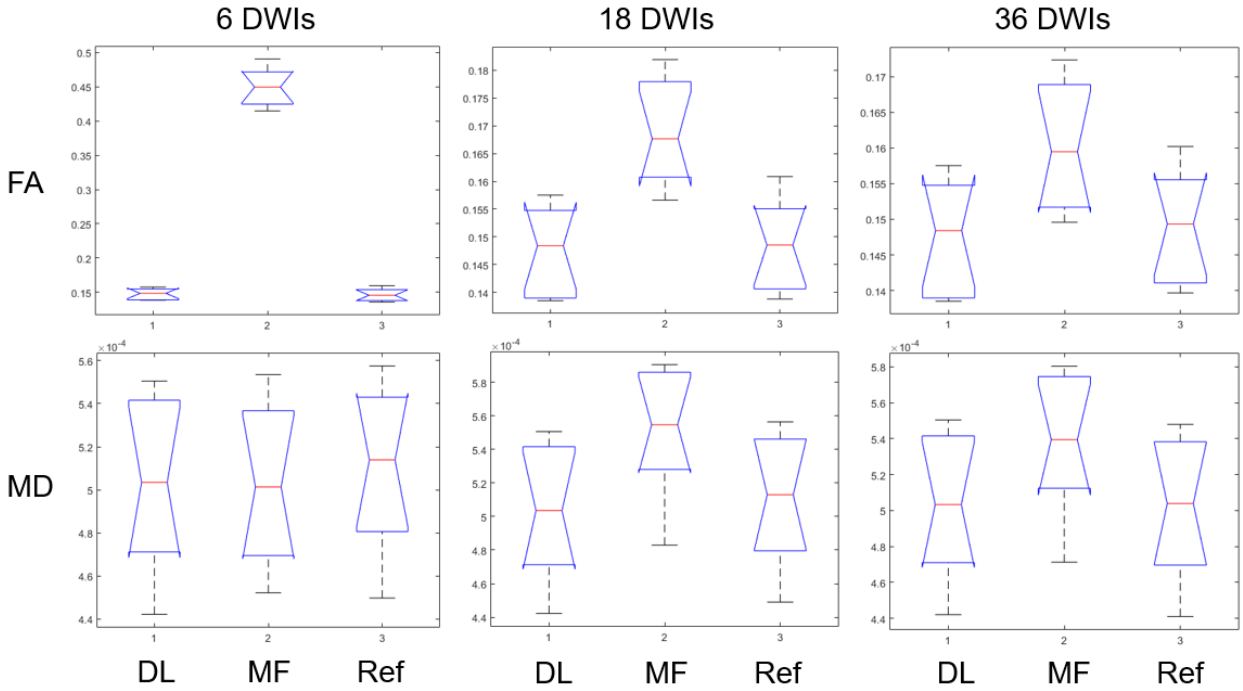


Fig. 7. ANOVA of proposed DL, MF and Reference for FA and MD. Left to right: results from 6, 18, and 36 DWIs.

III. STATISTICAL ANALYSES

For the HCP data, 10 sets of test images (a total of 1450 images) were used to evaluate the statistical accuracy of the FA and MD values estimated using the proposed DL and conventional MF methods. The Pearson correlation coefficient, student's t-test, and Analysis of Variance (ANOVA) results are summarized in Table I.

All statistical tests are two-tailed. Figure 7 also compares the ANOVA results of DL, MF estimates, and the reference.

The Pearson correlation test and t-test in Table I demonstrate the FA and MD results of the deep learning method using 6, 18, and 36 DWIs are statistically significant. The ANOVA results in Table I and Fig. 7 show the improvement of the deep learning method over the

model-fitting method is also statistically significant.

Lesion Detection in Stroke Patients.

DTI is known to benefit detection of white matter lesions. Our results demonstrate that the deep learning accelerated DTI acquisition preserve the ability to detect lesions even though the network was trained using data from normal subject. Figure 8 compares the FA maps obtained from six DWIs using the proposed

DL method and those from 30 DWIs with 2 averages using the conventional MF. The relative contrast of the lesion is shown on the bottom left corner of each image. It is seen that the FA map from 6 DWIs with DL can still reveal lesion with high contrast similar to that from 60 DWIs, while the MF with 10 DWIs fails to reveal the lesion. Although the training was performed on healthy volunteer data, the network still works for stroke patient data.

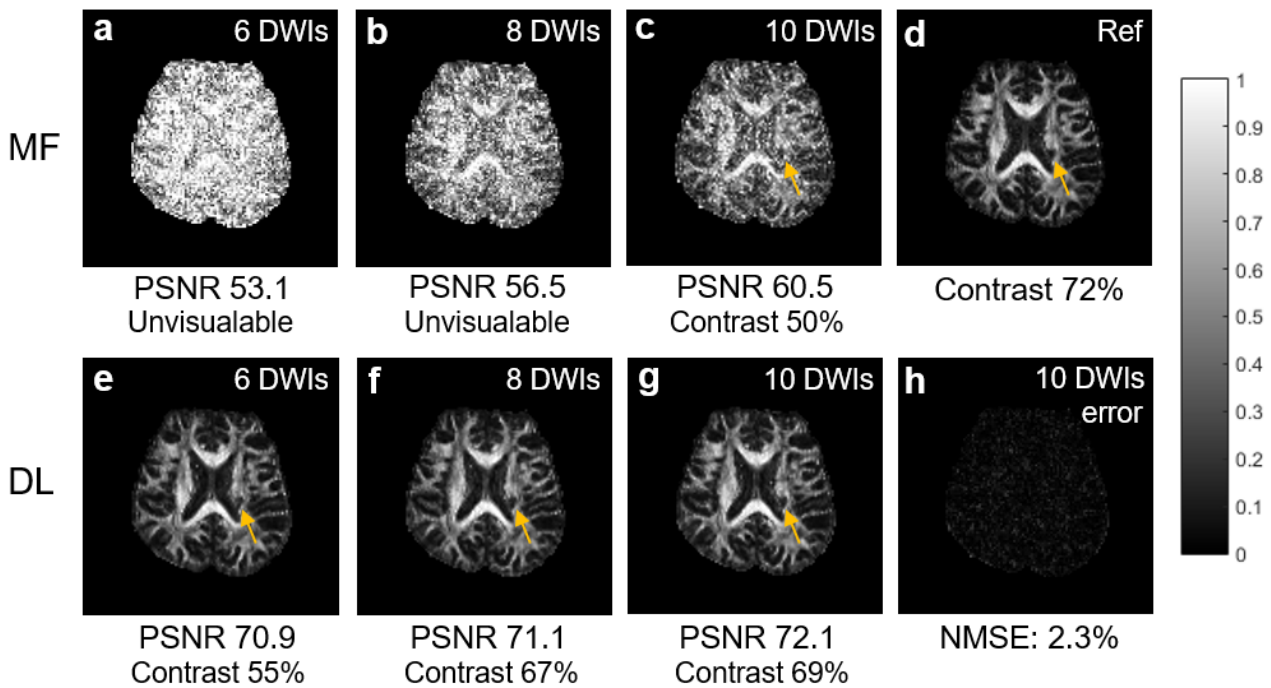


Fig. 8. Comparison of FA maps with lesion. Lesion maps were obtained from 6, 8, 10 DWIs using the conventional tensor model fitting (a-c), using proposed deep learning method (e-g). d, reference from 30 DWIs with 2 averages using the conventional tensor model fitting. h, difference map of 10 DWIs by proposed method.

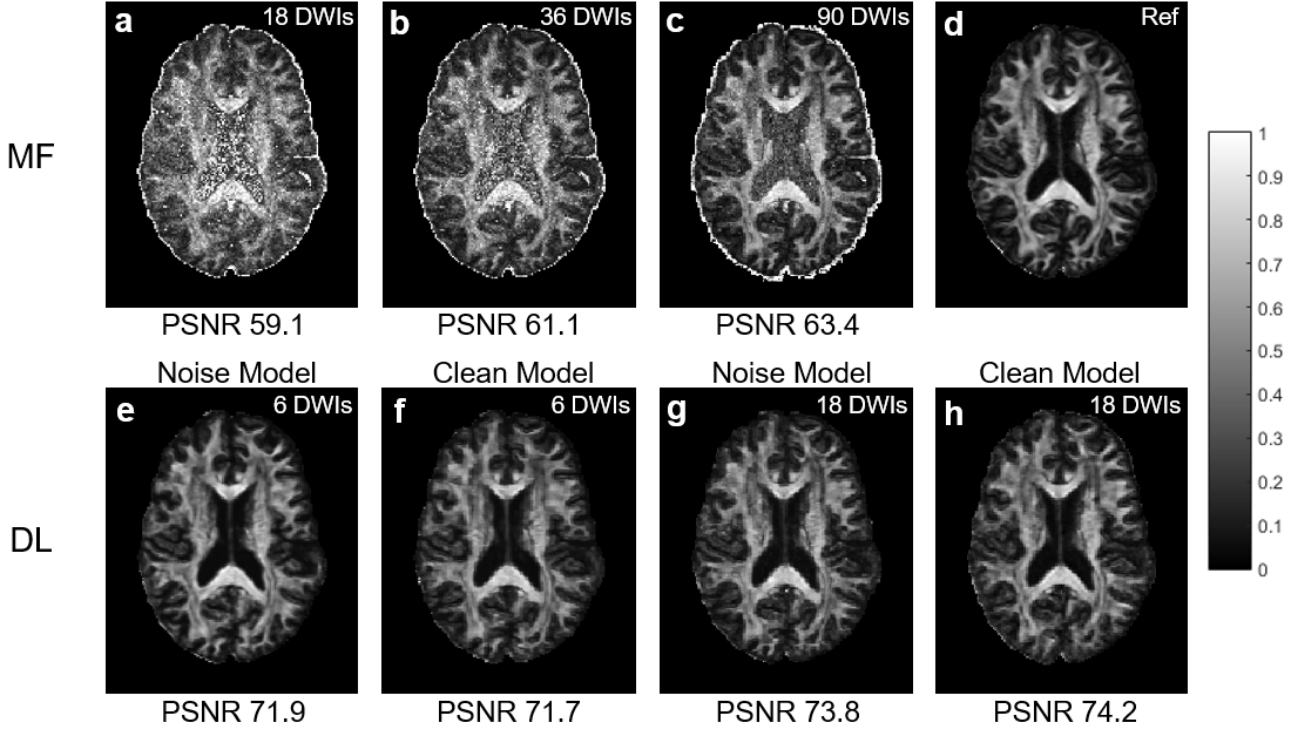


Fig. 9. FA maps with noisy input. The maps were generated from 18, 36, and 90 DWIs using conventional model-fitting (a-c); from 6 and 18 noisy DWIs using the proposed deep learning method (e-h). Noise model denotes noisy input for training and a clean model denotes clean one for training. The model-fitted FA map from 90 DWIs (d) is shown as reference.

IV. DISCUSSION

In order to study the noise robustness of our DL method and the conventional MF method, we added an additional 30db of white Gaussian noise to the diffusion-weighted images. As shown in Figure 9, the result shows that the conventional MF method fails to generate acceptable FA maps, even using 90 DWIs. In contrast, our DL method is still capable of generating FA maps close to the reference using as few as 6 DWIs. The training of the DL method is by using noisy DWIs as input, so it has the capability of de-noising. However, training with clean DWIs can also de-noise and recon accurate FA maps. The proposed DL method is robust to noise.

V. METHODS

A. Description of the deep learning algorithm

Our objective is to obtain the nonlinear mapping between q DWIs (input) and the FA, MD or FA color maps (output) using deep learning while by-passing the conventional tensor model. If the nonlinear mapping between the input x and the output y is represented as $y = F(x; \theta)$, where θ is the parameter that controls the nonlinear relationship, then a deep learning network is designed

such that the parameter θ can be learned to represent the true relationship through training faithfully.

A (de)convolutional neural network with L layers is used. Specifically, each of the $l = 1, \dots, L$ hidden layers calculates

$$H_l = \sigma_l(W_l * H_{l-1} + B_l) \quad (1)$$

for layers without skip connection, and

$$H_l = \sigma_l(W_l * (H_{l-1} + H_{L-l}) + B_l) \quad (2)$$

for layers with skip connection, where H_l is the output of layer l (H_0 stands for input), W_l and B_l represent the filters and biases respectively, ‘*’ denotes the (de)convolution operation, and σ_l the nonlinear operator (e.g., ReLU is used here). Here, W_l corresponds to n_l filters of support $n_{l-1} \times c \times c$, where n_{l-1} is the number of channels in the previous layer, c is the spatial size of a filter. We divide each image into many overlapping patches of size 21 by 21, and the filter size is 3 by 3. It is worth noting that although the filters have support in 3D, only 2D convolution with a $c \times c$ filter is actually performed and weighted sum of n_{l-1} channels is performed in the third dimension. The filter stride is set to one for all layers. Each patch instead of the whole image is used as a training sample. Except for the last layer, there are a total of $n_l = 64$ filters in each hidden

layer. For the first layer, the input of the network is the 2D patches of all q DWIs at the same spatial location (i.e., $n_0 = q$). For the last layer, the output of the network is the FA, MD ($n_L = 1$) or FA-weighted eigenvectors ($n_L = 3$) for that location. There are a total of five convolutional layers, followed by five deconvolutional layers in our implementation. The skip connection, originally introduced in ResNet [33], copies the early feature maps and reuses them as the input to a later layer of the same feature-map size in a network. Our network has four conveying paths, copying the output of an early convolutional layer and reusing it as the input to a later deconvolutional layer of the same feature-map size. Except for the last layer, each convolutional or deconvolutional layer is followed by a rectified linear unit (ReLU).

During training, both the input (DWIs) and output (ground truth FA, MD or colored FA) are given. The information is then used to train the filter weights and biases. Specifically, the objective is to minimize the loss function defined as the average mean squared error between the network prediction and the corresponding ground truth result for all training samples x^t and y^t :

$$L(\theta) = \frac{1}{n} \sum_{t=1}^n \|F(x^t; \theta) - y^t\|^2 \quad (3)$$

where $F(\cdot)$ represents the operation performed by the neural network. The optimization problem is solved by the backpropagation algorithm (implemented in Caffe [35]).

B. Human connectome project data

DWI data from a total of 50 subjects were randomly selected from the Human Connectome Project (HCP)[36]. The diffusion-weighted scans were collected using an HCP-specific variant of the multiband diffusion sequence. The diffusion MRI data were collected with 3 different gradient tables, each including 90 diffusion weighting directions, plus six $b = 0$ acquisitions. The diffusion directions were uniformly distributed on multiple q-space shells. The directions were optimized so that every subset of the first M directions is also isotropic. Each dataset includes 18 non-DWIs and 270 DWIs in three different b values: 1000, 2000, and 3000 s/mm^2 and 90 diffusion directions. Data from 40 subjects (145 slices for each subject, a total of 5,800 images) were used for training and the data from the rest 10 subjects were used for testing and statistical analysis.

C. Healthy volunteer and stroke patient data

The data used in this study were acquired previously in an ongoing trial (Identifier: NCT03163758) as described in [37, 38]. The study was approved by the ethics committee of the Peking Union Medical

College Hospital. We selected data from 10 healthy volunteers (5 males and 5 females, age 54.4 \pm 7.8 years) and 2 stroke patients (30 and 76 years old). The data from stroke patients were acquired within one year after onset. MRI data including DTI and structural images were acquired on a 3.0 T MRI scanner (MAGNETOM Skyra; Siemens, Erlangen, Germany) using a 20-channel phased-array head coil. DTI images were taken with a diffusion-weighted echo-planar imaging sequence (EPI) sequence. The DTI scan consisted of 30 diffusion-weighted directions with a b-value of 1000 s/mm^2 and one volume without diffusion weighting (i.e., b_0 image). The parameters of the DTI sequence were as follows: repetition time (TR) = 7900 ms, echo time (TE) = 94 ms, slice thickness = 2.5 mm, field of view (FOV) = 240 mm \times 240 mm, 60 axial slices with a slice thickness of 2.5 mm, slice gap 0.5 mm, matrix size = 122 \times 122, and two repetitions. Earplugs and earphones were used to reduce scan noises, and the head motion was minimized by stabilizing the head with cushions. Data from 10 healthy volunteers (a total of 600 images) were used for training, and the data from the two stroke patients were used for testing and analysis.

D. Data processing

The model-fitting results from all 90 directions of $b=1000$ s/mm^2 were used as the reference for the training of the DL network, calculation of MSE, and comparison of performance. When choosing a subset of the DWIs to generate the FA and MD maps using both DL and MF methods, the first $M=6, 18, \text{ or } 36$ diffusion directions were selected such that they are uniformly distributed on the q-space shell with $b=1000$ s/mm^2 .

MATRIX [39] was used to perform the conventional model fitting using the diffusion tensor model and to obtain the corresponding FA, MD, colored FA maps, and fiber tractography.

All testing images were segmented into 286 regions of interest (ROIs). The mean and MSE values of FA and MD in each ROI were calculated. Performance of DL with respect to MF in representative gray matter, major white matter, and subcortical white matter structures were examined.

The lesion contrast was calculated as the FA value difference between the lesion and the surrounding background normalized by the mean FA value of the background. Large values suggest better contrasts.

E. Statistical Metrics

The Pearson correlation coefficient is calculated using

$$r = \frac{\sum_{i=1}^n (x_i - \bar{x})(y_i - \bar{y})}{\sqrt{\sum_{i=1}^n (x_i - \bar{x})^2} \sqrt{\sum_{i=1}^n (y_i - \bar{y})^2}} \quad (4)$$

where $n = 10$ is used here as the sample size, x_i, y_i are the FA (or MD) values averaged over all the image for the i^{th} reconstruction and reference, respectively, $i = 1, 2, \dots, 10$, and \bar{x}, \bar{y} are the corresponding mean over all samples. For student's t-test, the t-value is calculated as

$$t = \frac{\bar{x} - \bar{y}}{s_p \sqrt{\frac{2}{n}}} \quad (5)$$

where s_p is an estimator of the pooled standard deviation of the two samples.

The ANOVA compares the variation between groups to the variation within groups. The test statistic has an F-distribution with $(k - 1, N - k)$ degrees of freedom, and the F value is defined as

$$F = \frac{SSR/(k-1)}{SSE/(N-k)} \sim F_{k-1, N-k} \quad (6)$$

where $k = 10, N = 3, SSR = \sum_{j=1}^3 n_j (\bar{y}_j - \bar{y})^2$ is the variation of group mean from the overall sample mean, where $\bar{y}_j, i = 1, 2, 3$ are the FA (or MD) values averaged over all the image from DL reconstruction, traditional model fitting and reference, respectively, and \bar{y} is the corresponding mean over all samples. $SSE = \sum_{j=1}^3 \sum_{i=1}^{10} (\bar{y}_{ij} - \bar{y}_j)^2$ is the variation of the observations within each group \bar{y}_{ij} from their group mean \bar{y}_j .

REFERENCES

- Moseley, M.E., et al., *Diffusion-weighted MR imaging of anisotropic water diffusion in cat central nervous system*. Radiology, 1990. **176**(2): p. 439-445.
- Le, D.B., *Molecular diffusion nuclear magnetic resonance imaging*. Magnetic resonance quarterly, 1991. **7**(1): p. 1-30.
- Bammer, R., *Basic principles of diffusion-weighted imaging*. European journal of radiology, 2003. **45**(3): p. 169-184.
- Moseley, M., et al., *Diffusion-weighted MR imaging of acute stroke: correlation with T2-weighted and magnetic susceptibility-enhanced MR imaging in cats*. American Journal of Neuroradiology, 1990. **11**(3): p. 423-429.
- Lansberg, M.G., et al., *Advantages of adding diffusion-weighted magnetic resonance imaging to conventional magnetic resonance imaging for evaluating acute stroke*. Archives of neurology, 2000. **57**(9): p. 1311-1316.
- Larsson, H., et al., *In vivo magnetic resonance diffusion measurement in the brain of patients with multiple sclerosis*. Magnetic resonance imaging, 1992. **10**(1): p. 7-12.
- Horsfield, M.A., et al., *Apparent diffusion coefficients in benign and secondary progressive multiple sclerosis by nuclear magnetic resonance*. Magnetic resonance in medicine, 1996. **36**(3): p. 393-400.
- Christiansen, P., et al., *Increased water self-diffusion in chronic plaques and in apparently normal white matter in patients with multiple sclerosis*. Acta neurologica scandinavica, 1993. **87**(3): p. 195-199.
- Nakahara, M., K. Ericson, and B. Bellander, *Diffusion-weighted MR and apparent diffusion coefficient in the evaluation of severe brain injury*. Acta Radiologica, 2001. **42**(4): p. 365-369.
- Sundgren, P., et al., *Value of conventional, and diffusion-and perfusion weighted MRI in the management of patients with unclear cerebral pathology, admitted to the intensive care unit*. Neuroradiology, 2002. **44**(8): p. 674-680.
- Stadnik, T.W., et al., *Diffusion-weighted MR imaging of intracerebral masses: comparison with conventional MR imaging and histologic findings*. American Journal of Neuroradiology, 2001. **22**(5): p. 969-976.
- Kono, K., et al., *The role of diffusion-weighted imaging in patients with brain tumors*. American journal of neuroradiology, 2001. **22**(6): p. 1081-1088.
- Sundgren, P., B. Edvardsson, and S. Holtås, *Serial investigation of perfusion disturbances and vasogenic oedema in hypertensive encephalopathy by diffusion and perfusion weighted imaging*. Neuroradiology, 2002. **44**(4): p. 299-304.
- Hinchey, J., et al., *A reversible posterior leukoencephalopathy syndrome*. New England Journal of Medicine, 1996. **334**(8): p. 494-500.
- Basser, P.J., J. Mattiello, and D. LeBihan, *Estimation of the effective self-diffusion tensor from the NMR spin echo*. Journal of Magnetic Resonance, Series B, 1994. **103**(3): p. 247-254.
- Moseley, M.E., et al., *Anisotropy in diffusion-weighted MRI*. Magnetic Resonance in Medicine, 1991. **19**(2): p. 321-326.
- Pierpaoli, C. and P.J. Basser, *Toward a quantitative assessment of diffusion anisotropy*. Magnetic resonance in Medicine, 1996. **36**(6): p. 893-906.
- Song, S.-K., et al., *Diffusion tensor imaging detects and differentiates axon and myelin degeneration in mouse optic nerve after retinal ischemia*. Neuroimage, 2003. **20**(3): p.

- 1714-1722.
19. Mac Donald, C.L., et al., *Diffusion tensor imaging reliably detects experimental traumatic axonal injury and indicates approximate time of injury*. Journal of Neuroscience, 2007. **27**(44): p. 11869-11876.
 20. Krissian, K., G. Malandain, and N. Ayache. *Directional anisotropic diffusion applied to segmentation of vessels in 3D images*. in *International Conference on Scale-Space Theories in Computer Vision*. 1997. Springer.
 21. Lu, H., et al., *Three - dimensional characterization of non - gaussian water diffusion in humans using diffusion kurtosis imaging*. NMR in Biomedicine: An International Journal Devoted to the Development and Application of Magnetic Resonance In vivo, 2006. **19**(2): p. 236-247.
 22. Tuch, D.S., et al., *High angular resolution diffusion imaging reveals intravoxel white matter fiber heterogeneity*. Magnetic Resonance in Medicine: An Official Journal of the International Society for Magnetic Resonance in Medicine, 2002. **48**(4): p. 577-582.
 23. Barth, M., et al., *Simultaneous multislice (SMS) imaging techniques*. Magnetic resonance in medicine, 2016. **75**(1): p. 63-81.
 24. Landman, B.A., et al., *Resolution of crossing fibers with constrained compressed sensing using diffusion tensor MRI*. NeuroImage, 2012. **59**(3): p. 2175-2186.
 25. Menzel, M.I., et al., *Accelerated diffusion spectrum imaging in the human brain using compressed sensing*. Magnetic Resonance in Medicine, 2011. **66**(5): p. 1226-1233.
 26. Wu, Y., et al., *Accelerated MR diffusion tensor imaging using distributed compressed sensing*. Magnetic resonance in medicine, 2014. **71**(2): p. 763-772.
 27. Michailovich, O., Y. Rathi, and S. Dolui, *Spatially regularized compressed sensing for high angular resolution diffusion imaging*. IEEE transactions on medical imaging, 2011. **30**(5): p. 1100-1115.
 28. Landman, B.A., et al. *Resolution of crossing fibers with constrained compressed sensing using traditional diffusion tensor MRI*. in *Medical Imaging 2010: Image Processing*. 2010. International Society for Optics and Photonics.
 29. Shi, X., et al., *Parallel imaging and compressed sensing combined framework for accelerating high - resolution diffusion tensor imaging using inter - image correlation*. Magnetic resonance in medicine, 2015. **73**(5): p. 1775-1785.
 30. Golkov, V., et al., *Q-space deep learning: twelve-fold shorter and model-free diffusion MRI scans*. IEEE transactions on medical imaging, 2016. **35**(5): p. 1344-1351.
 31. Krizhevsky, A., I. Sutskever, and G.E. Hinton. *Imagenet classification with deep convolutional neural networks*. in *Advances in neural information processing systems*. 2012.
 32. Yasaka, K., et al., *Deep learning with convolutional neural network in radiology*. Japanese journal of radiology, 2018. **36**(4): p. 257-272.
 33. He, K., et al. *Deep residual learning for image recognition*. in *Proceedings of the IEEE conference on computer vision and pattern recognition*. 2016.
 34. Xu, L., et al. *Deep convolutional neural network for image deconvolution*. in *Advances in neural information processing systems*. 2014.
 35. Jia, Y., et al. *Caffe: Convolutional architecture for fast feature embedding*. in *Proceedings of the 22nd ACM international conference on Multimedia*. 2014. ACM.
 36. Van Essen, D.C., et al., *The Human Connectome Project: a data acquisition perspective*. Neuroimage, 2012. **62**(4): p. 2222-2231.
 37. Li, J., et al., *Cerebral functional reorganization in ischemic stroke after repetitive transcranial magnetic stimulation: an fMRI study*. CNS neuroscience & therapeutics, 2016. **22**(12): p. 952-960.
 38. Guan, Y.Z., et al., *Effectiveness of repetitive transcranial magnetic stimulation (rTMS) after acute stroke: A one - year longitudinal randomized trial*. CNS neuroscience & therapeutics, 2017. **23**(12): p. 940-946.
 39. Tournier, J.D., F. Calamante, and A. Connelly, *MRtrix: diffusion tractography in crossing fiber regions*. International journal of imaging systems and technology, 2012. **22**(1): p. 53-66.

Data Availability

The HCP datasets used are available in the Human Connectome Project repository, <http://www.humanconnectomeproject.org/data/>. The stroke patients and control used in this study are not publicly available due to HIPPA policy but might be available from the corresponding author on reasonable request.

Acknowledgments

This work is supported in part by the National Institute of Health Brain Initiative R01EB025133.

Author Contributions

L.Y. J. Z. and Y. G. conceived the project. H. L. developed deep learning algorithms and generated the results. J. L. and W. Z. designed and performed MRI experiments for healthy subjects and stroke patients. C. Z. and R. L. generated the results from the conventional method. H. L. analyzed the data. Z. L. and J. Z. interpreted the data. L.Y. and J.Z. wrote the manuscript. All authors discussed the results and commented on the manuscript.

Competing Financial Interests

The authors declare no competing financial interests.